Slow crack growth resistance of electrically conductive zirconia-based composites with non-oxide reinforcements

Fei Zhang[a,b*], Jérôme Chevalier[b], Christian Olagnon[b], Shuigen Huang[a], Wout Veulemans[a], Kim Vanmeensel[a] and Jef Vleugels[a]

[a] KU Leuven, Department of Materials Engineering, Kasteelpark Arenberg 44, B-3001 Heverlee, Belgium

[b] Univ. Lyon, UMR CNRS 5510 (MATEIS), INSA de Lyon, France

* E-mail address: fzfei.zhang@hotmail.com; fei.zhang@kuleuven.be

Abstract

Slow crack growth (SCG) behavior of four zirconia-based composites reinforced with 40 vol% WC, TiC, NbC or TiCN were studied by means of double-torsion testing. Compared to monolithic zirconia, the composites had a higher resistance to fast fracture, i.e., higher fracture toughness. The extent of toughening depended on the reinforcement type, shifting the V-K_I (crack velocity versus stress intensity factor) curve parallel to higher K_I values. More importantly, these composites were less sensitive to SCG. Identical V-K_I/K_{IC} curves with steeper slopes compared to monolithic zirconia were observed for the investigated composites, independent on the reinforcement type. No rising R-curve was measured, at least in the crack-size domain investigated by SCG. Therefore, the higher SCG resistance of the composites was due to the intrinsic stress-assisted corrosion resistance of the covalent non-oxide secondary phase.

Key words: Fracture resistance; Slow crack growth; Zirconia; Non-oxide reinforcements;

1. Introduction

Zirconia-based composites have been widely explored to develop materials with high toughness and strength thanks to the phase transformation toughening effect [1]. Nevertheless, zirconia, as an oxide ceramic, is prone to chemically-assisted Slow Crack Growth (SCG). Water molecules can be adsorbed to the strained Zr-O-Zr bonds at the crack tip or any pre-existing defect in the material and initiate the crack propagation in a subcritical manner [2, 3]. By 'subcritical', it means that crack growth can occur at a stress intensity (K_I) below the 'critical' stress intensity factor, i.e. fracture toughness (K_{IC}), degrading the load-bearing capacity of ceramic materials over time and resulting in premature failure. 3Y-TZP (3 mol% yttria-stabilized) zirconia ceramics for example can exhibit substantial crack growth at stress intensity factors as low as 50% of K_{IC} [2]. Therefore, SCG is one of the important limitations of oxide ceramics for structural applications, particularly in the presence of water-containing environments.

On the other hand, machining of ceramics is a big challenge. Reinforcing with a conductive phase increases the electrical conductivity, allowing the use of electrical discharge machining (EDM) as a component shaping technology [4, 5] and providing some additional functions like the use of the conductive character to self-monitor crack extensions [6]. The electrically conductive materials commonly used are transition metal carbides, nitrides, borides or carbonitrides [7], such as WC [8, 9], TiCN [4, 10], TiN [11], ZrB_2 [12], NbC [13] or TiC [14, 15], allowing the electrically conductive material to be accurately shaped into very complex parts, irrespective of their strength or hardness. These additional phases should have an effect

on the crack resistance of the ceramic and especially on SCG since non-oxide ceramics are generally considered to be less sensitive to stress-assisted corrosion by water [16, 17].

However, to the best of the authors' knowledge, the SCG behavior of zirconia-based composites with electro-conductive reinforcements or non-oxide additives has not been assessed. The goal of this study is to investigate the crack resistance (mainly the subcritical crack growth) of zirconia-based composites with different non-oxide reinforcements.

2. Materials and Methods

Four ZrO_2-based composites with 40 vol% NbC, TiN, WC or TiCN, referred to as ZrO_2-NbC, ZrO_2-TiN, ZrO_2-WC and ZrO_2-TiCN, were studied. The zirconia matrix phase in ZrO_2-NbC, ZrO_2-WC, ZrO_2-TiN and ZrO_2-TiCN contained 3, 2, 1.75 and 1.75 mol% yttria stabilizer, respectively. 0.8 wt.% alumina of the whole composite was added in all the composites as sintering aid [8, 10, 11]. In order to optimize the zirconia phase transformability in the different composite materials, the yttria content was adjusted depending on the reinforcement phase, so that an optimal fracture toughness could be combined with avoidance of spontaneous transformation after sintering [4, 8, 10, 11, 18]. A monolithic zirconia (3 mol% yttria-stabilized tetragonal zirconia with 0.05 wt% alumina addition – Tosoh Zpex®, Japan), referred to as ZrO_2, was used as reference ceramic.

The starting powders of the four zirconia-based composites were prepared by mixing the appropriate amount of pure monoclinic ZrO_2 powder (TZ-0 grade, Tosoh, Japan, particle size 27 nm), 3 mol% yttria co-precipitated ZrO_2 powder (HSY-3U, Daiichi, Japan, crystal size 30 nm or TZ-3Y, Tosoh, Japan, crystal size 27 nm), alumina (Baikowski SM8, France, crystal size 0.6 µm or TM-DAR, Taimei Chemicals Co., Ltd, Nagano, Japan) and non-oxide reinforcements (WC: MBN J550 Mechanomade nanocrystalline 20 nm powder agglomerates < 10 µm; TiCN: H.C. Starck grade B, de-agglomerated particles with a crystal size of 3-5 µm, the ratio of C/N is 5/5; TiN: Kennametal Jetmilled, USA, crystal size 1.03 µm; NbC: Seco, Sweden, 300 nm particle size). The mixing was performed on a multidirectional mixer (Turbula) in ethanol for 24 h. The ethanol was removed in a rotating evaporator at 65°C and the powders were dried in a furnace at 90°C for 24 h. The dried powders were sieve granulated (325 µm) after drying.
ZrO_2-WC, ZrO_2-TiC and ZrO_2-TiCN were made by hot-pressing (W100/150-2200-50 LAX, FCT Systeme, Germany) in vacuum (~ 10 Pa) at 1450°C for 2 h under a mechanical load of 28 MPa. ZrO_2-NbC was prepared by spark plasma sintering (Type HP D25/1, FCT Systeme, Frankenblick, Germany) in vacuum at 1450°C for 5 min under a maximum pressure of 30 MPa. The reference ZrO_2 was obtained by cold isostatic pressing (250 MPa) of the starting powder and pressureless sintering in air at 1450°C for 2 h. Since the goal of this study was to assess the crack growth behavior, more details on the powder preparation and sintering process can be found elsewhere [4, 8, 10, 11, 18].

The density was measured according to the Archimedes principle in ethanol. Scanning electron microscopy (SEM, XL-30FEG, FEI, Eindhoven, The Netherlands) was used to characterize the microstructure of polished surfaces. The Vickers hardness (Model FV-700, Future-Tech Corp., Tokyo, Japan) was measured with a load of 98 N (n=10/each grade). The flexural strength at room temperature was measured in a 3-point bending test (Instron 4467, PA, USA) with a span length of 20 mm (n=10/each grade). The dynamic Young's modulus was measured using the resonance frequency method by the impulse excitation technique (Model Grindo-Sonic, J. W. Lemmens N.V., Leuven, Belgium). The electrical resistance was measured according to the 4-point contact method using a Resistomat (TYP 2302 Burster, Gernsbach, Germany).

The crack growth resistance was assessed by measuring the relationship between the crack growth velocity (V) and the stress intensity factor (K_I) by means of the double torsion method. Testing was performed under static loading conditions at room temperature in ambient air (~50% RH). The double-torsion (DT) plates had a dimension of 40×20×2 mm^3. Details on specimen geometry and loading configuration are provided elsewhere [3, 19]. The tensile surface was polished with diamond pastes down to 1 μm in order to facilitate crack observation. A notch of length $a_0 \approx 10$ mm was machined using a 0.3 mm width diamond sawing blade. Two Vickers indentations were made ahead of the notch tip to initiate a small crack. Subsequent pre-cracking was performed by slowly loading the specimens at a rate of 10 μm/min to induce a real shape crack with an initial length a_i of 12-13 mm, with a crack tip far enough from the initial indentations created to initiate a real crack from the notch.

The load relaxation was performed to obtain the V-K_I diagram in the velocity range of 10^{-2}-10^{-7} m/s [20, 21]. Pre-cracked specimens were loaded at a constant rate of 0.3 mm/min to a certain load and then the crosshead was stopped at constant displacement to obtain the load relaxation with time. The crack velocity (V) was calculated using the following equation [20]:

$$V = -\frac{P_f}{P^2}\left(a_f + \frac{D}{B}\right)\left(\frac{dP}{dt}\right) \quad (1)$$

with a_f the final crack length, P_f the final load, and dP/dt the relaxation slope at a given time, D/B is the constant from the compliance calibration.

The applied stress intensity (K_I) for the double torsion configuration was calculated according to the following expression [2, 20]:

$$K_I = \frac{W_m}{T^2}\left[\frac{3(1+\nu)}{W\psi}\right]^{1/2} P\left(\frac{a}{a_0}\right)^{6/32} \quad (2)$$

with W_m the span length, T the sample thickness, W the sample width, ν the Poisson ratio (taken equal to 0.25), ψ a calibration factor [19], P the applied load, a the total crack length on the tensile surface, and a_0 the notch length.

The fracture toughness (K_{IC}) was determined from the V-K_I curves at a crack rate of about 10^{-3} m/s (fast fracture region), which also corresponds to small crack extension (just after pre-cracking). In addition, since the crack-resistance curve (R-curve) can play an important role in SCG [22], R-curve and compliance analysis were also performed on pre-cracked DT samples. Load-displacement curves with a series of loading-unloading sequences in the crack range of 10-30 mm were accurately followed at a constant speed of 10 μm/min using a linear variable differential transformer (LVDT). The load at which the crack propagates was determined and K_R was calculated using equation (2). The crack length was directly measured using optical microscopy after each unloading of the specimen during the test. This method of obtaining a long-crack R-curve and the use of unloading compliance have been used in many studies [23-26]. The details are explained in [22, 26].

The failure behavior and microstructure were investigated using scanning electron microscopy (SEM, XL-30FEG, FEI, Eindhoven, The Netherlands) on DT specimens. In particular, the crack propagation mode at the crack tip (crack velocity of about 10^{-6} m/s) was emphasized. The crack plane of the double torsion samples after fracture was analyzed by XRD to estimate the amount of stress-induced transformation. The analysis was performed by grazing-incidence XRD to obtain information of the upper 2 μm surface layer. The monoclinic zirconia (m-ZrO_2) volume fraction was calculated according to the formula of Toraya et al [27] and Garvie et al [28].

3. Results

Table 1 summarizes the general properties of the investigated composites including hardness, bending strength, fracture toughness evaluated from the DT tests, Young's modulus and electrical conductivity. As reported before, the 40 vol % addition of secondary NbC, WC, TiC or TiCN phase resulted in better mechanical properties (hardness, strength as well as fracture toughness) and also converted the electrical insulating zirconia matrix into an electrically conductive composite [4, 8, 10, 11, 18]. The electrical resistivity threshold for EDM is between 100 and 300 Ω·cm [29], so these composites can be machined by wire and die sinking electrical discharge machining.

The slow crack growth behavior of the reference ZrO_2 and the four composites is compared in Figure 1. Similar to the monolithic zirconia ceramic, the V-K_I diagrams of the composite materials had three regions with a fast fracture (region III) and slow crack growth (region I and II). The addition of TiCN, TiN, WC and NbC non-oxide phases not only shifted the curves to higher K_I values but also increased the slope, implying a higher resistance to fast fracture and SCG.

The reproducibility of the results was checked on at least two specimens for each material, revealing a deviation of about 0.5 $MPa \cdot m^{1/2}$ on the K_I values. From equation (2), the uncertainty on the K_I value mainly originated from the accuracy of the sample thickness (± 0.02 mm) and recorded load (± 0.5 N), resulting in a ~5% uncertainty on the reported K_I. Considering this accuracy on the K_I value, the fracture toughness of ZrO_2-TiCN ≅ ZrO_2-WC > ZrO_2-TiN > ZrO_2-NbC > ZrO_2.

In the SCG region, i.e., the crack growth at K_I levels below the K_{IC}, the V-(K_I/K_{IC}) curves were plotted by normalizing to their respective fracture toughness values in Figure 2. Interestingly, the V-(K_I/K_{IC}) curves of the four composites were the same, yet significantly different compared to the curve of the monolithic zirconia. The curves corresponding to the composites exhibited steeper slopes. Stage II occurred at a lower crack growth rate and spread over a narrower K_I range. Therefore, NbC, TiN, WC and TiCN addition significantly increased the resistance to SCG and premature failure.

Regarding the crack resistance curves shown in Figure 3, flat R-curves were observed for all the composites. The accompanying compliance analysis (Figure 4) confirmed that there was no significant bridging effect existing in the investigated composites. In the presence of crack bridging elastic ligaments, the compliance would be strongly deviating from the linear relationship [30], which was not the case in the present study. Crack surface observations (Figure 5) confirmed that there was no clear crack bridging effect. The microstructures of the studied composites were fine grained (Figure 6) and the crack propagated not only through the zirconia phase but also through the reinforcement phases.

4. Discussion

4.1. Toughening and fracture toughness, K_{IC}

The critical stress intensity factor (fracture toughness, K_{IC}) of the materials in general consists of intrinsic and extrinsic toughening contributions. Since extrinsic toughening is the primary toughening source of brittle materials, the fracture toughness normally is described as [1, 31]:

$$K_R = K_{IC} = K_0 + \Delta K_c \quad (3)$$

With K_0, the intrinsic matrix toughness and ΔK_c the extrinsic toughening in the wake of the crack from various crack-shielding mechanisms that mainly include crack deflection, crack bridging and transformation toughening.

Crack bridging in general is a potent toughening mechanism, but was not observed in the investigated materials (Figure 4 and Figure 5), because the reinforcements were brittle intermetallic compounds with an equiaxed morphology. Crack deflection was observed in all composites (Figure 5), which however is known to be less effective, especially when small-grain size is concerned. Therefore, transformation toughening should be the most effective toughening mechanism in the investigated composites, i.e., $K_{IC} = K_0 + \Delta K_{cT}$ where ΔK_{cT} is commonly given by [1]:

$$\Delta K_{cT} = \frac{\eta E^* e_T V_f h^{1/2}}{1 - \upsilon} \quad (4)$$

With η a factor depending on the zone shape at the tip and the nature of the stress field in that zone, E^* the effective modulus of the material, e_T the lattice dilatation associated to the transformation (about 5%), V_f the transformed volume fraction of particles, h the width of the transformation zone and ν the Poisson ratio.

In the present study, the matrix of all composites is yttria-stabilized zirconia, so the η, e_T and ν values are expected to be similar and the main difference in ΔK_{cT} originates from E^* and $V_f h^{1/2}$. The difference in $V_f h^{1/2}$ (transformability) results from the different yttria stabiliser content, the residual tensile thermal stresses induced by the secondary phase and the constraint of the reinforcement phase with higher E modulus. The thermal expansion coefficient of the non-oxide reinforcements (8.6, 5.2-5.92, 9.4 and 6.6-7.4 x 10^{-6}/K for TiCN, WC, TiN and NbC phase, respectively) is smaller than for zirconia (9.8-10.2 x 10^{-6}/K), resulting in residual tensile stresses during cooling after sintering. The E-modulus of TiCN, WC, TiN and NbC phase is about 473, 652-686, 471, 420-480 GPa, respectively, which is higher than that of ZrO_2 matrix (195-210 GPa) and constrain the phase transformation [11, 32-37]. It is also noteworthy that although the nitrides and carbides are brittle, their different intrinsic toughness can have a multiplicative effect and influence the transformation zone size ($h^{1/2}$) [38]. Since the E, V_f, $h^{1/2}$, K_0 and ΔK_{CT} parameters are interactive in a composite system, it is difficult to accurately quantitatively estimate the ΔK_{CT} values. Nevertheless, the transformability ($V_f h^{1/2}$) of a zirconia-based material can be experimentally evaluated from the difference in m-ZrO_2 content measured on the fracture surface of a crack plane and the as-sintered surface (see amount of stress induced m-ZrO_2 in Table 1 and Figure 7). Note that the peak of m-ZrO_2 at 31.4° 2θ overlaps with a WC peak in the ZrO_2-WC composite, so the intensity of the peak at 31.4° 2θ was not included in the formula of Toraya et al [27] to calculate the m-ZrO_2 fraction in all the materials. Although the resulting values do not precisely represent the m-ZrO_2 fraction on the fracture surface of the crack plane, it allows comparison of the transformation toughening efficiency in the different materials. Overall, the transformability of ZrO_2-WC ≥ ZrO_2-TiCN > ZrO_2-TiN > ZrO_2-NbC > ZrO_2, which agrees well with fracture toughness trend. No attempt was made in this work to fit a universal equation to the K_{IC} of the investigated composites, but the above description shows that the active toughening mechanism in the present composites is mainly stress-induced transformation toughening.

4.2. Slow crack growth

The addition of 40 vol % non-oxide reinforcement (NbC, TiN, WC or TiCN) phases resulted in a V-K_I/K_{IC} curve with steeper slope and a narrower K_I range, i.e., higher resistance to SCG.

Depending on the crack length, the rising part of R-curve could result in a higher slope of the V-K_I curve [22]. In the present work however, flat R-curves were measured for all the composites, so all the active toughening mechanisms operate at short length crack scale, which agrees with the transformation toughening behavior of yttria-stabilized zirconia with

transformation zone of only several micrometers [39]. The R-curve of the reference pure 3Y-TZP zirconia ceramic was reported to steeply increase and reach the plateau at a crack length below 10 μm [39, 40]. Therefore, all the DT measurements performed in this work were conducted under the steady state conditions of the R-curve. Therefore, the higher SCG resistance of the composites should be attributed to the intrinsic properties of the covalent ceramic additives, which are known to be less sensitive to water-assisted stress-corrosion cracking [16, 17, 41, 42]. Note that the steady-state K_R values obtained from the R-curve are lower than the K_{IC} values obtained from the V-K_I test, due to the fact that R-Curve data were obtained with an applied crosshead rate of 10 μm/s, leading to K_I values corresponding to crack rates of about $2x10^{-5}$ m/s.

The SCG susceptibility of zirconia ceramics, like other oxides, is associated to the reaction between strained Zr-O-Zr bonds and water molecules (or other corrosive species like ammonia or polar solvents) [2, 3, 16]. The reaction involves: (1) adsorption of water molecules to the Zr-O-Zr bonds; (2) water molecules donating electrons and protons to zirconium and the linking oxygen, respectively; (3) formation of Zr-O-H hydroxyl bonds in combination with the rupture of Zr-O-Zr bonds [3, 16]. In terms of the three-stage V-K_I curve measured in air, stage I is ruled by this water-induced bond rupture reaction. As K_I increases, the diffusion rate of water molecules from the crack mouth to the crack tip becomes the limiting mechanism (Stage II). The crack velocity in stage II is thus controlled by the diffusion of water molecules to the reaction site. Stage III is associated with fast fracture, corresponding to the commonly reported K_{IC}, as discussed in section 4.1. Since stage I and stage II are sensitive to water-assisted stress corrosion, they should indeed be affected by the water-affinity of the materials, as observed in this work. The NbC, TiN, WC and TiCN phases are free of oxygen bonds and less sensitive to bond rupture reaction by water molecules than oxide ceramics [41, 42]. Therefore, the composites have a lower sensitivity to SCG, which is reflected in a higher slope of the V-K_I/K_{IC} curves. The stress corrosion susceptibility coefficient (n) of stage I and stage II were estimated from the V-K_I curves by fitting with the form $V = A(\frac{K_I}{K_{IC}})^n$, as summarised in Table 2, Higher n values were obtained for the composite materials. Monolithic zirconia ceramics normally exhibit substantial crack growth at stress intensity factors as low as 50% of the K_{IC} [2]. In contrast, the SCG in the investigated composites starts around 70% of the K_{IC}. Covalent ceramics, such as SiC and Si_3N_4, are almost insensitive to SCG with a very high slope in the V-K_I/K_{IC} diagrams [17, 41, 42]. It is also expected that the water-sensitivity of the nitride, carbide and carbonitride phases are similar, explaining why the V-(K_I/K_{IC}) curve is independent on the type of non-oxide reinforcement at a constant secondary phase content of 40 vol%.

Conclusions

Reinforcing zirconia ceramics with 40 vol % of electrically conducting transition metal carbides (WC, NbC), nitrides (TiN) or carbonitrides (TiCN) is promising to fabricate structural materials with an excellent crack growth resistance in terms of fast fracture (fracture toughness, K_{IC}, stage III) as well as water-assisted slow crack growth (stage I and Stage II).

The higher toughness of the composite materials was mainly attributed to their higher transformation toughening behavior, resulting in a parallel shift of the V-K_I curves to higher K_{IC} values at a flat R-curve behavior. More importantly, due to the presence of non-oxide reinforcements, the composites were less sensitive to stress corrosion by water molecules with a concomitantly higher resistance to slow crack growth. The V-K_I curves of the composites had steeper slopes and spread out over a narrower K_I range compared to the monolithic Y-TZP ceramic.

Acknowledgements

F. Zhang thanks the Fund for Scientific Research Flanders (FWO-Vlaanderen) for her post-doctoral fellowship (12S8418N). The JECS-Trust is acknowledged for travel grant No. 201599, which allowed performing double torsion testing in the MATEIS lab of INSA, Lyon, France.

Tables:

Table 1. Properties of electrically conductive zirconia-based composites [4, 8, 10, 11, 18].

	ZrO_2	**ZrO_2-NbC**	**ZrO_2-TiN**	**ZrO_2-WC**	**ZrO_2-TiCN**
Density (g/cm^3)	6.05	6.15	5.81	9.80	5.76
HV_{10} (GPa)	13.4 ± 0.2	14.2 ± 0.1	13.7 ± 0.1	16.9 ± 0.1	14.2 ± 0.1
Bending strength (MPa)	1276 ± 98	1435 ± 71	1674 ± 314	1964 ± 88	1521 ± 61
E-modulus (GPa)	209 ± 2	293 ± 10	290 ± 7	328 ± 2	284 ± 10
Electrical resistivity (10^{-6} Ω·m)	Insulator	14.3	4.6	4.3	17
Fracture toughness ($MPa \cdot m^{1/2}$) DT	5.1 ± 0.5	5.7 ± 0.5	7.0 ± 0.5	8.0 ± 0.5	8.4 ± 0.5
m-ZrO_2 after sintering (vol%)	0	2	6	5	5
Stress-induced m-ZrO_2* (vol.%)	7 ± 1	17 ± 1	33 ± 3	50 ± 1	42 ± 3

Notes: (1) The reported values are average value ± standard deviation; (2) ∗m-ZrO_2 content on the fracture surface of double torsion crack plane minus the m-ZrO_2 content on as-sintered samples.

Table 2. The stress corrosion susceptibility coefficient (n) in air

	ZrO_2	**ZrO_2-NbC**	**ZrO_2-TiN**	**ZrO_2-WC**	**ZrO_2-TiCN**
Stage I	27 ± 6	47 ± 8	68 ± 12	75 ± 15	55 ± 10
Stage II	4 ± 1	9 ± 1	10 ± 1	10 ± 1	11 ± 1

Figures

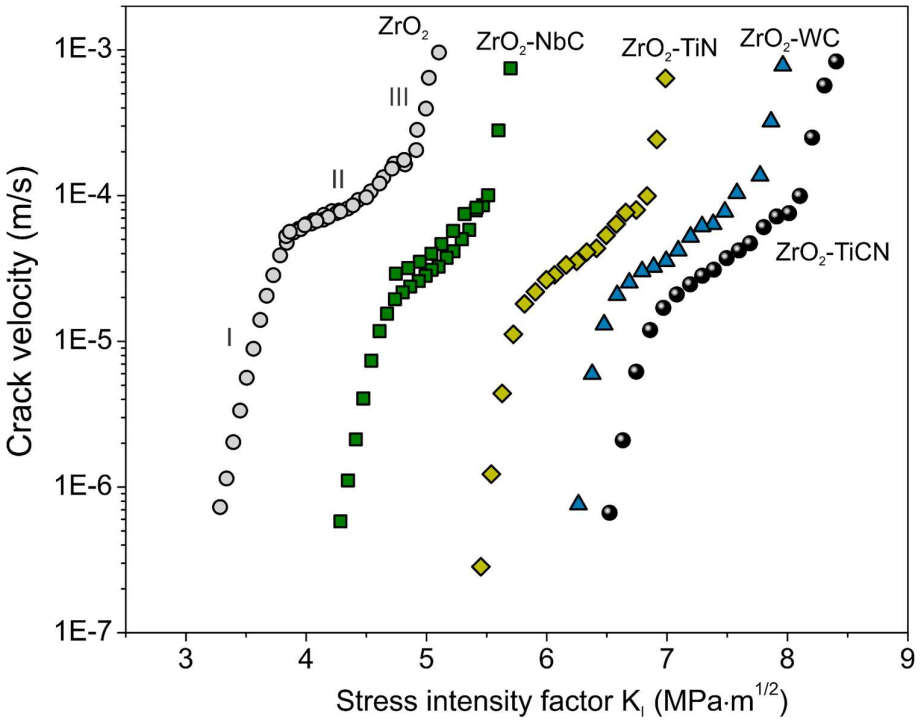

Figure 1. V-K_I diagrams.

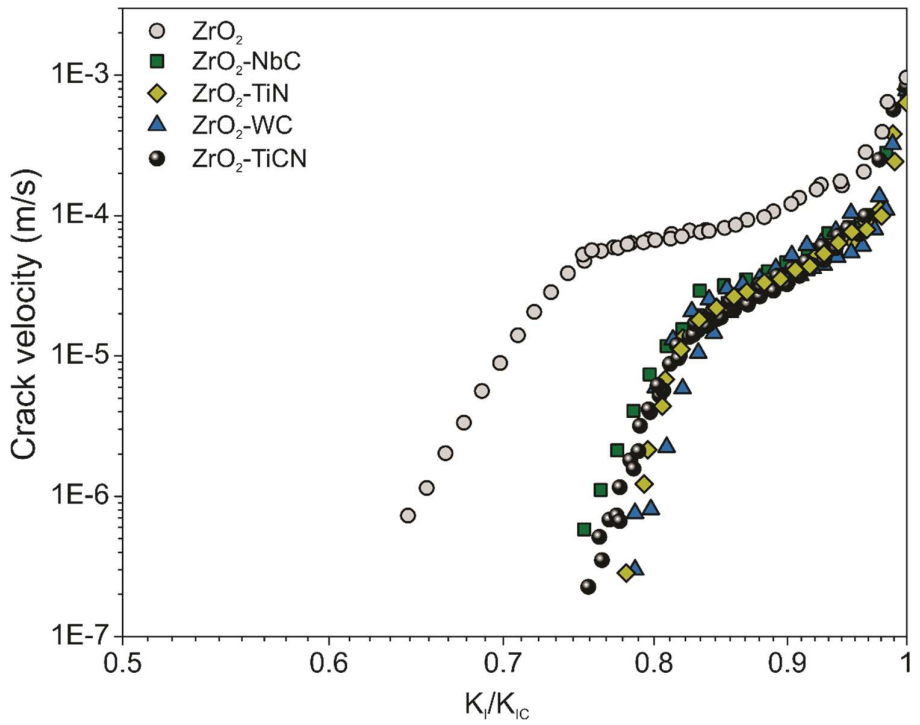

Figure 2. V-K_I/K_{IC} diagrams.

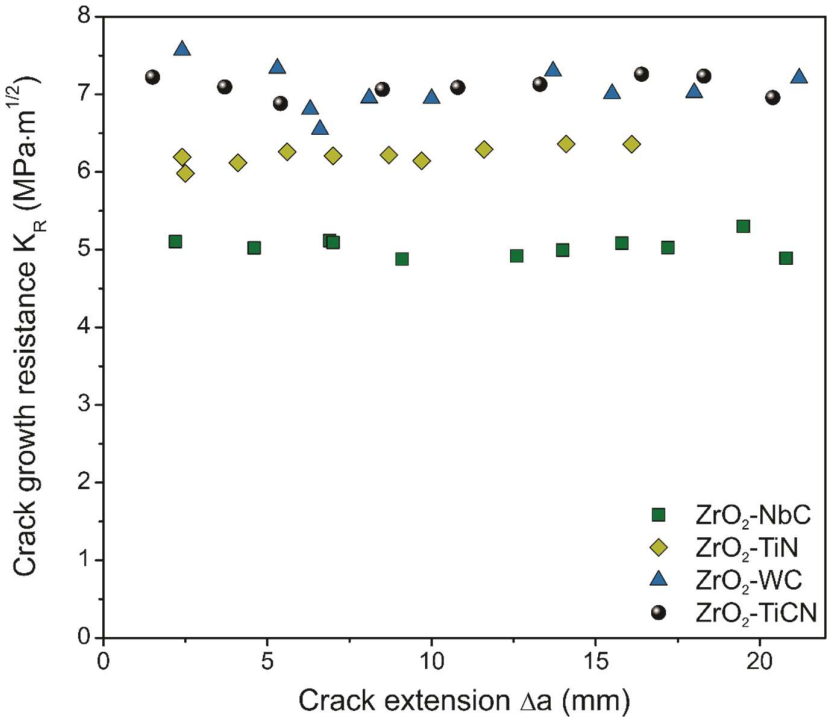

Figure 3. R-curve versus crack extension.

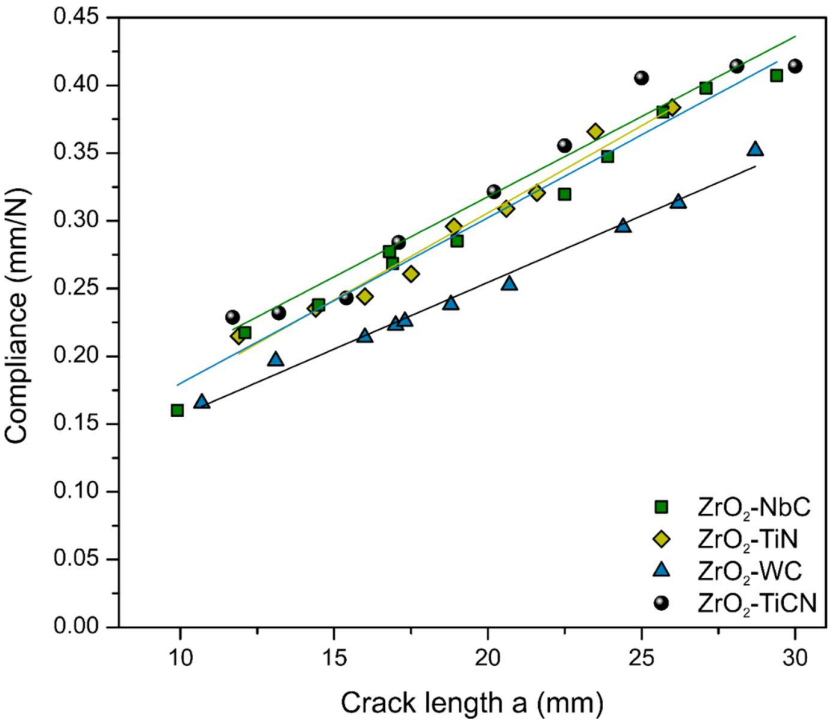

Figure 4. Compliance of the DT specimen versus crack length.

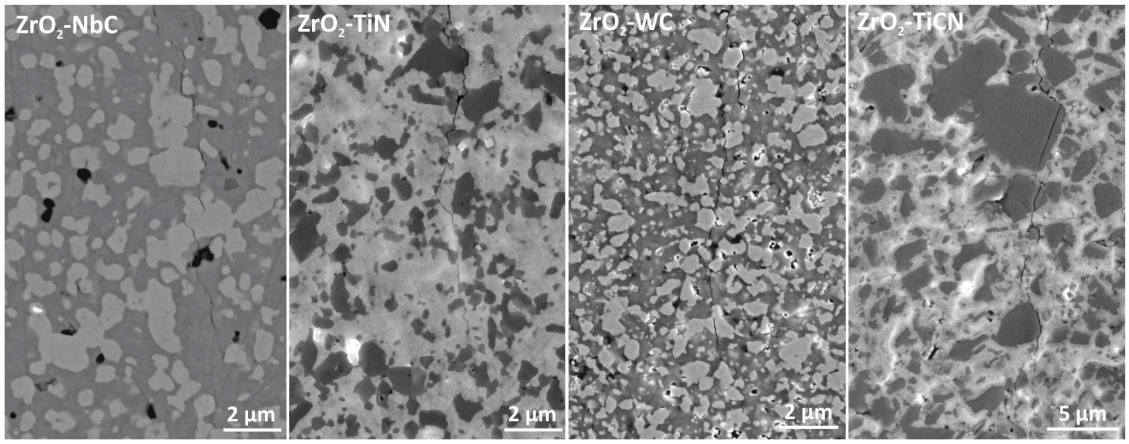

Figure 5. Crack-tip (sharp, natural cracks) propagation on the DT specimen surface: ZrO_2-NbC (bright), ZrO_2-TiN (dark), ZrO_2-WC (bright) and ZrO_2-TiCN (dark).

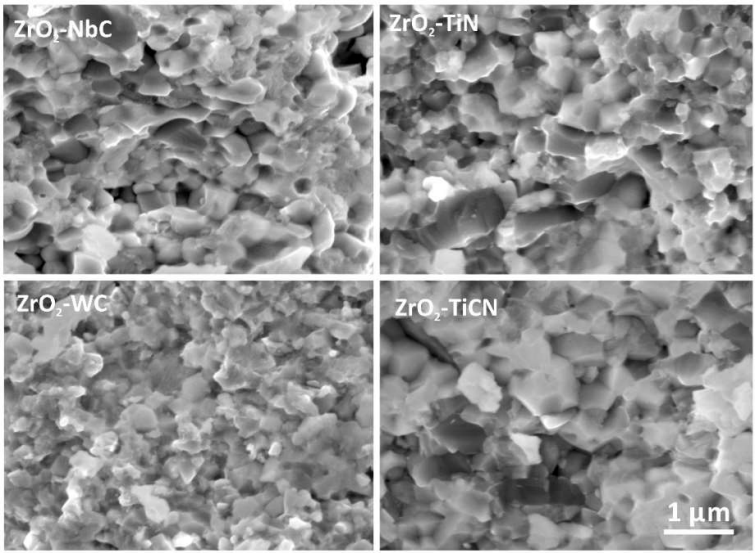

Figure 6. DT specimen fracture surface of the four composites.

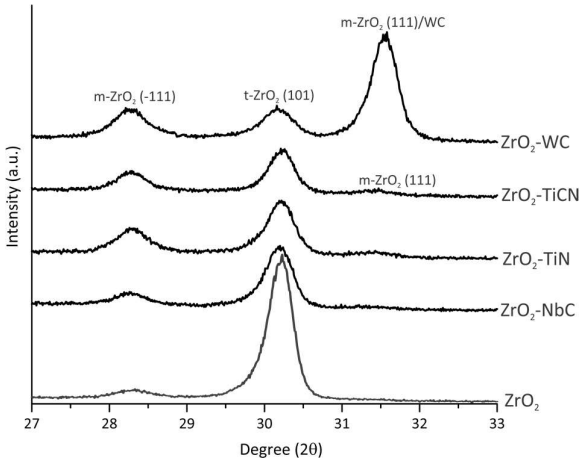

Figure 7. Grazing-incidence XRD patterns recorded from the fracture surface of the double torsion crack plane.

References

[1] R.H.J. Hannink, P.M. Kelly, B.C. Muddle, Transformation Toughening in Zirconia-Containing Ceramics, Journal of the American Ceramic Society 83(3) (2000) 461-487.
[2] J. Chevalier, C. Olagnon, G. Fantozzi, Subcritical Crack Propagation in 3Y-TZP Ceramics: Static and Cyclic Fatigue, Journal of the American Ceramic Society 82(11) (1999) 3129-3138.
[3] A.H. De Aza, J. Chevalier, G. Fantozzi, M. Schehl, R. Torrecillas, Crack growth resistance of alumina, zirconia and zirconia toughened alumina ceramics for joint prostheses, Biomaterials 23(3) (2002) 937-945.
[4] K. Bonny, P. De Baets, J. Vleugels, A. Salehi, O. Van der Biest, B. Lauwers, W. Liu, Influence of secondary electro-conductive phases on the electrical discharge machinability and frictional behavior of ZrO2-based ceramic composites, Journal of Materials Processing Technology 208(1–3) (2008) 423-430.
[5] B. Lauwers, K. Brans, W. Liu, J. Vleugels, S. Salehi, K. Vanmeensel, Influence of the type and grain size of the electro-conductive phase on the Wire-EDM performance of ZrO2 ceramic composites, CIRP Annals - Manufacturing Technology 57(1) (2008) 191-194.
[6] O.T. Picot, V.G. Rocha, C. Ferraro, N. Ni, E. D'Elia, S. Meille, J. Chevalier, T. Saunders, T. Peijs, M.J. Reece, E. Saiz, Using graphene networks to build bioinspired self-monitoring ceramics, Nature Communications 8 (2017) 14425.
[7] C. Kral, W. Lengauer, D. Rafaja, P. Ettmayer, Critical review on the elastic properties of transition metal carbides, nitrides and carbonitrides, Journal of Alloys and Compounds 265(1–2) (1998) 215-233.
[8] D. Jiang, O. Van der Biest, J. Vleugels, ZrO2–WC nanocomposites with superior properties, Journal of the European Ceramic Society 27(2–3) (2007) 1247-1251.
[9] G. Anné, S. Put, K. Vanmeensel, D. Jiang, J. Vleugels, O. Van der Biest, Hard, tough and strong ZrO2–WC composites from nanosized powders, Journal of the European Ceramic Society 25(1) (2005) 55-63.
[10] J. Vleugels, O. Van der Biest, Development and Characterization of Y2O3-Stabilized ZrO2 (Y-TZP) Composites with TiB2, TiN, TiC, and TiC0.5N0.5, Journal of the American Ceramic Society 82(10) (1999) 2717-2720.
[11] S. Salehi, O. Van der Biest, J. Vleugels, Electrically conductive ZrO2–TiN composites, Journal of the European Ceramic Society 26(15) (2006) 3173-3179.
[12] F. Monteverde, A. Bellosi, S. Guicciardi, Processing and properties of zirconium diboride-based composites, Journal of the European Ceramic Society 22(3) (2002) 279-288.
[13] U. Schmitt-Radloff, F. Kern, R. Gadow, Spark plasma sintering and hot pressing of ZTA-NbC materials – A comparison of mechanical and electrical properties, Journal of the European Ceramic Society 38(11) (2018) 4003-4013.
[14] P. Ninz, R. Landfried, F. Kern, R. Gadow, Electrical discharge machining of metal doped Y-TZP/TiC nanocomposites, Journal of the European Ceramic Society 35(14) (2015) 4031-4037.
[15] R. Landfried, F. Kern, W. Burger, W. Leonhardt, R. Gadow, Development of Electrical Discharge Machinable ZTA Ceramics with 24 vol% of TiC, TiN, TiCN, TiB2 and WC as Electrically Conductive Phase, International Journal of Applied Ceramic Technology 10(3) (2013) 509-518.
[16] B. Lawn, Fracture of Brittle Solids, second Edition Cambridge: Cambridge University Press1993.
[17] C. Olagnon, J. Chevalier, V. Pauchard, Global description of crack propagation in ceramics, Journal of the European Ceramic Society 26(15) (2006) 3051-3059.
[18] K. Bonny, P. De Baets, J. Vleugels, O. Van der Biest, A. Salehi, W. Liu, B. Lauwers, Reciprocating sliding friction and wear behavior of electrical discharge machined zirconia-

based composites against WC–Co cemented carbide, International Journal of Refractory Metals and Hard Materials 27(2) (2009) 449-457.
[19] A. Shyam, E. Lara-Curzio, The double-torsion testing technique for determination of fracture toughness and slow crack growth behavior of materials: A review, Journal of Materials Science 41(13) (2006) 4093-4104.
[20] D. Williams, A. Evans, A Simple Method for Studying Slow Crack Growth, (1973) 264-270.
[21] J. Chevalier, M. Saadaoui, C. Olagnon, G. Fantozzi, Double-torsion testing a 3Y-TZP ceramic, Ceramics International 22(2) (1996) 171-177.
[22] M.E. Ebrahimi, J. Chevalier, G. Fantozzi, Slow crack-growth behavior of alumina ceramics, Journal of Materials Research 15(1) (2000) 142-147.
[23] R.W. Steinbrech, A. Reichl, W. Schaarwächter, R-Curve Behavior of Long Cracks in Alumina, Journal of the American Ceramic Society 73(7) (1990) 2009-2015.
[24] E.H. Lutz, M. Sakai, R-Curve and Compliance Change upon Renotching, Journal of the American Ceramic Society 76(12) (1993) 3113-3122.
[25] M. Jenkins, J. Mikami, T. Chang, A. Okura, A Fracture Resistance Measurement Procedure for Brittle Materials, Transactions of the Japan Institute of Metals 29(7) (1988) 573-579.
[26] G. Vekinis, M.F. Ashby, P.W.R. Beaumont, R-curve behaviour of Al2O3 ceramics, Acta Metallurgica et Materialia 38(6) (1990) 1151-1162.
[27] H. Toraya, M. Yoshimura, S. Somiya, Calibration Curve for Quantitative Analysis of the Monoclinic-Tetragonal ZrO_2 System by X-Ray Diffraction, Journal of the American Ceramic Society 67(6) (1984) C-119-C-121.
[28] R.C. Garvie, P.S. Nicholson, Phase Analysis in Zirconia Systems, Journal of the American Ceramic Society 55(6) (1972) 303-305.
[29] W. König, D.F. Dauw, G. Levy, U. Panten, EDM-Future Steps towards the Machining of Ceramics, CIRP Annals - Manufacturing Technology 37(2) (1988) 623-631.
[30] M.E. Ebrahimi, J. Chevalier, G. Fantozzi, R-curve evaluation and bridging stress determination in alumina by compliance analysis, Journal of the European Ceramic Society 23(6) (2003) 943-949.
[31] L.M. E., R.R. O., On the Fracture Toughness of Advanced Materials, Advanced Materials 21(20) (2009) 2103-2110.
[32] CES EDuPack (2016).
[33] H.O. Pierson, 5 - Carbides of Group V: Vanadium, Niobium and Tantalum Carbides, Handbook of Refractory Carbides and Nitrides, William Andrew Publishing, Westwood, NJ, 1996, pp. 81-99.
[34] R. Morrell, Handbook of Properties of Technical & Engineering Ceramics, An Introduction for Engineer and Designer (Part1). HSMO, London and Norwich (1985) 95–166.
[35] H.O. Pierson, 11 - Interstitial Nitrides: Properties and General Characteristics, Handbook of Refractory Carbides and Nitrides, William Andrew Publishing, Westwood, NJ, 1996, pp. 181-208.
[36] S. Cardinal, A. Malchère, V. Garnier, G. Fantozzi, Microstructure and mechanical properties of TiC–TiN based cermets for tools application, International Journal of Refractory Metals and Hard Materials 27(3) (2009) 521-527.
[37] G.M. Zheng, J. Zhao, Y.H. Zhou, Z.J. Gao, Preparation and Characterization of Si3N4/TiCN Composite Ceramic Tool Material, Advanced Materials Research 152-153 (2011) 500-503.
[38] P.F. Becher, T.N. Tiegs, Toughening Behavior Involving Multiple Mechanisms: Whisker Reinforcement and Zirconia Toughening, Journal of the American Ceramic Society 70(9) (1987) 651-654.

[39] J. Eichler, M. Hoffman, U. Eisele, J. Rödel, R-curve behaviour of 2Y-TZP with submicron grain size, Journal of the European Ceramic Society 26(16) (2006) 3575-3582.
[40] K. Yoshida, F. Wakai, N. Nishiyama, R. Sekine, Y. Shinoda, T. Akatsu, T. Nagoshi, M. Sone, Large increase in fracture resistance of stishovite with crack extension less than one micrometer, Scientific Reports 5 (2015) 10993.
[41] J. Chevalier, S. Deville, G. Fantozzi, J.F. Bartolomé, C. Pecharroman, J.S. Moya, L.A. Diaz, R. Torrecillas, Nanostructured Ceramic Oxides with a Slow Crack Growth Resistance Close to Covalent Materials, Nano Letters 5(7) (2005) 1297-1301.
[42] N. Al Nasiri, N. Ni, E. Saiz, J. Chevalier, F. Giuliani, L.J. Vandeperre, Effect of microstructure and grain boundary chemistry on slow crack growth in silicon carbide at ambient conditions, Journal of the European Ceramic Society 35(8) (2015) 2253-2260.